

Analysis of spatial emission structures in vertical-cavity surface-emitting lasers with feedback of a volume Bragg grating

Y. Noblet and T. Ackemann*
*SUPA, Department of Physics, University of Strathclyde,
107 Rottenrow, Glasgow G4 0NG, Scotland, UK*

We investigate the spatial and spectral properties of broad-area vertical-cavity surface-emitting lasers (VCSEL) with frequency-selective feedback by a volume Bragg grating (VBG). We demonstrate wavelength locking similar to the case of edge-emitters but the spatial mode selection is different from the latter. On-axis spatial solitons obtained at threshold give way to off-axis extended lasing states beyond threshold. The investigations focus on a self-imaging external cavity. It is analyzed how deviations from the self-imaging condition affect the pattern formation and a certain robustness of the phenomena is demonstrated.

PACS numbers: 42.55.Px, 42.60.Jf, 42.65.Sf, 42.60.Da, 42.65.Tg

I. INTRODUCTION

Volume Bragg gratings (VBG) are compact, narrow-band frequency filters which prove to be of increasing use in photonics. One particular application is the wavelength control of edge-emitting laser diodes (EEL), where they can stabilize the emission wavelength very effectively against the red-shift connected to an increase of ambient temperature or to the Ohmic heating due to increasing current [1–3]. In addition, the spectral and spatial brightness of broad-area EEL can be reduced significantly by the feedback from a VBG [1, 2]. Commercial versions are referred to as ‘wavelength-locker’ or ‘power-locker’.

Frequency-selective feedback was proposed and demonstrated to provide some control of transverse modes also for vertical-cavity surface-emitting lasers (VCSEL), both for medium-sized devices emitting Gaussian modes [4, 5] as well as for broad-area devices emitting Fourier modes [6]. These investigations used diffraction gratings and to our knowledge the only investigations using VBG were performed with a focus on the close-to-threshold region where bistable spatial solitons are formed [7, 8]. In this work, we are reporting experiments on how the solitons formed at threshold give way to spatially extended spatial structures and analyze their properties quantitatively. We will discuss similarities and differences to the edge-emitting case and to what extent VBG are helpful to control spatial modes in a VCSEL. We are focusing on a specific setup of the external cavity close to a self-imaging situation and analyze how deviations from the self-imaging condition are influencing the pattern formation.

II. EXPERIMENTAL SETUP

A schematic diagram of the experimental setup is illustrated in Fig. 1. The VCSEL used for this experiment is fabricated by Ulm Photonics and similar to the ones described in more detail in [6, 7, 9, 10]. It is a large aperture device, allowing for the formation of many transverse cavity modes of fairly high order, with a 200 μm diameter circular oxide aperture providing optical and current guiding. The emission takes place through the n-doped Bragg reflector and through a transparent substrate (so-called bottom-emitter, [9, 10]). The laser has an emission wavelength around 975 nm at room temperature. The VCSEL is tuned in temperature up to 70 °C so the emission wavelength approaches the reflection peak of the volume Bragg grating (VBG). The VBG has a reflection peak at $\lambda_g = 981.1$ nm with a reflection bandwidth of 0.2 nm full-width half-maximum (FWHM). At such a high temperature the free running laser nearly has an infinite threshold and lasing only occurs because of the feedback from the VBG.

The VCSEL is coupled to the VBG via a self-imaging external cavity. Every point of the VCSEL is imaged at the same spatial position after each round trip therefore maintaining the high Fresnel number of the VCSEL cavity. The VCSEL is collimated by $f_1 = 8$ mm focal length plano-convex aspheric lens. The second lens is a $f_2 = 50$ mm focal length plano-convex lens and is used to focus the light onto the VBG. This telescope setup gives a 6.25 : 1 magnification factor onto the VBG. This cavity has a round trip frequency of 1.23 GHz which corresponds to a round trip time of 0.81 ns. The light is coupled out of the cavity using a glass plate (beam splitter with a front uncoated facet and a back anti reflection coated facet). The reflection is relying on Fresnel reflection and therefore is polarization dependent. The reflectivity is on the order of 10 % for s-polarized light and 1 % for p-polarized light.

An optical isolator is used to prevent reflection from the detection to pass into the external cavity. There are two charge-coupled-device (CCD) cameras used for de-

* thorsten.ackemann@strath.ac.uk

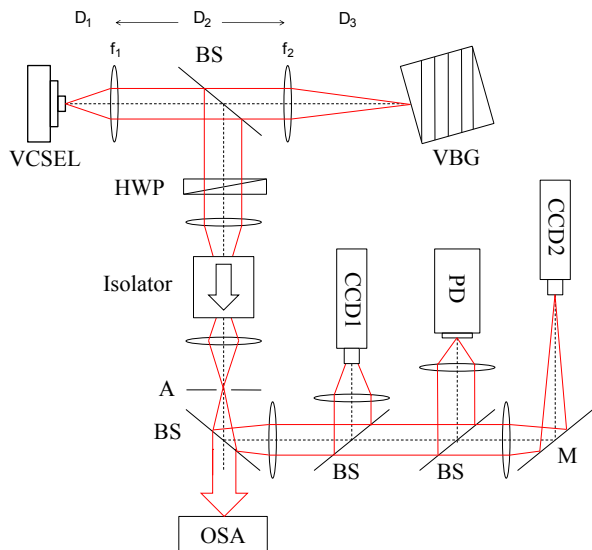


FIG. 1. Experimental setup. VCSEL: Vertical-cavity surface-emitting laser, BS: Beamsplitter, VBG: Volume Bragg grating, HWP: Half wave plate, A: Aperture, M: Mirror, PD: Photodiode, CCD1: CCD camera in near field image plane of VCSEL, CCD2: CCD camera in far field image plane of VCSEL, OSA: Optical spectrum analyzer.

tection, one is used to produce images of the VCSEL gain region (near field) and the other camera produces images of the Fourier plane of the gain region (far field). The emission spectrum is recorded with an optical spectrum analyzer (OSA). There is also a photodiode which measures the laser power.

The spontaneous emission is rather homogeneous below threshold (Fig. 2a) but as the current increases the intensity becomes higher at the boundaries due to current crowding at the oxide aperture [10]. In spite of the large aperture the device is still capable of lasing at low enough temperatures. The lower the temperature the lower the current required to achieve lasing. Above threshold the laser starts to lase on a kind of whispering gallery mode (e.g. [11]) around the boundaries of the VCSEL (Fig. 2b). The gain is the highest due to the current crowding previously observed therefore leading to a lower threshold of this mode.

III. EXPERIMENTAL RESULTS

A. Alignment of self-imaging cavity

As indicated, the cavity consists of two lenses forming an astronomical telescope. Thus the magnification factor M of this telescope is determined by the ratio of the two focal lengths. The position of the first lens, D_1 , is adjusted to provide the best collimation of the VCSEL output. The distance between the two intra-cavity lenses, D_2 should be $f_1 + f_2$ for an afocal telescope, where f_1

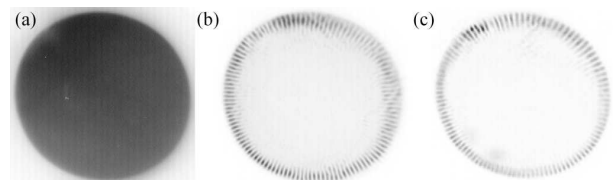


FIG. 2. Near field intensity distribution of the VCSEL showing a) spontaneous emission at $I = 200$ mA (at a temperature of 70°C) without feedback (this, and all other images in this article, depict intensity in a linear gray scale with black denoting high intensity); b) VCSEL without feedback, $I = 490$ mA at $T = 16^\circ\text{C}$; c) VCSEL with feedback from a plane mirror, $I = 185$ mA at $T = 70^\circ\text{C}$. Note that the slight non-homogenous behavior of the spontaneous emission (decrease of intensity from the upper left to the lower right) is due to the detection setup.

and f_2 are the two focal lengths of both lenses. In reality this is difficult to adjust because the lenses are ‘thick’. We started with an approximate placement given by the nominal focal lengths but improved this as discussed later in Sect. V. (The data given in Figs. 2c and 3 correspond to the optimized position.) The position of the VBG (or the mirror) closing the cavity at D_3 is determined from images like in Fig. 3 obtained at high current. When the boundaries of the aperture are sharp and well defined this is supposedly the self-imaging position (compare the left (and right) column to the two central ones). We remark that the telescope is still imaging the intensity distribution for correct D_1 , D_3 but incorrect D_2 (see the discussion around Eq. 4 later), but that for self-imaging of intensity and phase profiles, D_2 needs to equal $f_1 + f_2$.

B. Feedback with a mirror

For completeness, we study first the case of feedback with a plane mirror, i.e. without frequency selection. The laser starts at a quite low threshold of around 170 mA. The emission (Fig. 2c) is characterized by a ring with fringes perpendicular to the aperture and this is very similar to what we observe with the free running laser at lower temperature. Obviously, this preference for the perimeter is again a gain effect due to the current crowding.

If the current is increased, the inner part of the lasing aperture starts to lase also but a certain preference for the perimeter stays (upper image, right column, Fig. 3). A blow-up of a characteristic structure is shown in Fig. 4c. If the current is increased further the output power increases further but the spatial structure stays essentially the same (lower images, right column, Fig. 3). The emission in far field (Fig. 5, right column) is quite broad with a disk-shaped structure on axis surrounded by a faint halo (right column, Fig.5). At the transition between center and halo, one wavenumber is somewhat enhanced leading to a ring (left column, Fig.5). This wavenumber is

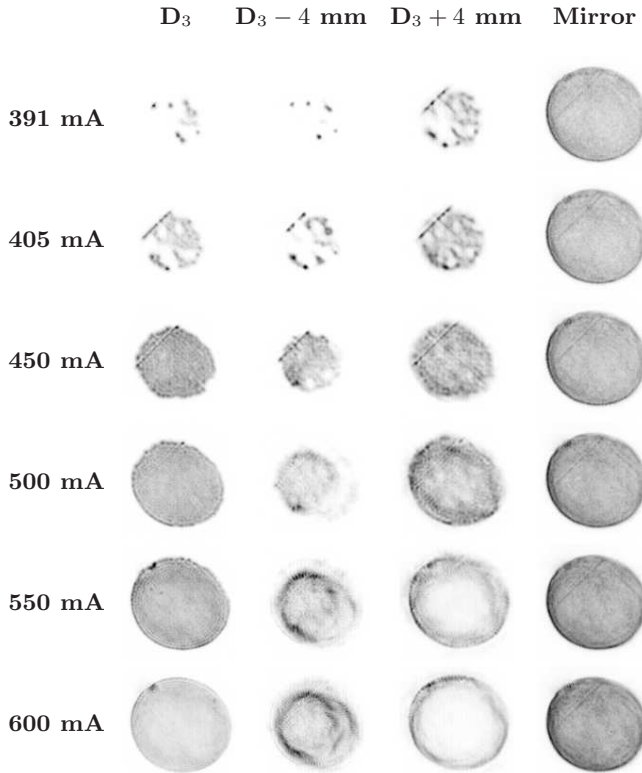


FIG. 3. Near field intensity distribution of the VCSEL with feedback from a VBG at different currents. Left column: D_3 at self-imaging distance; center columns: D_3 too short or too large by 4 mm; right column: Feedback with plane mirror.

probably favored by the detuning between the frequency of the gain maximum and the longitudinal cavity resonance as discussed before for free-running devices of this kind [11].

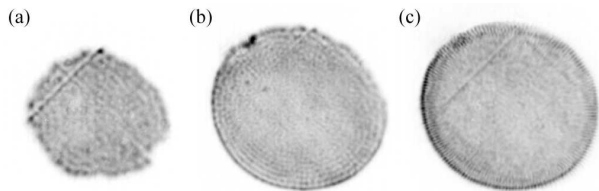


FIG. 4. Near field intensity distribution of the VCSEL with feedback from a VBG (a,b) and a plane mirror (c). a, c) $I = 450$ mA, b) $I = 550$ mA.

C. Feedback with VBG

With the VBG the threshold is much higher and at threshold small localized spots spontaneously appear in the near field of the laser, away from the boundaries (left column, uppermost image in Fig. 3). These spots are the laser cavity solitons (LCS) investigated in [7, 8, 12]. If the current is increased further, more LCS appear at other

locations and LCS already formed give way to extended lasing states of lower amplitude (images in left column of Fig. 3). At about 500 mA essentially the whole aperture is lasing, whereas with the mirror this is already the case for about 400 mA. The patterns are actually quite similar to the ones obtained with a plane mirror, i.e., fine waves at high spatial frequency filling up the whole aperture of the device. However, there is the important difference that the length scale now depends on current: As a comparison between the blow-ups in Fig. 4a and b shows, the wavelength of these waves decreases with increasing current.

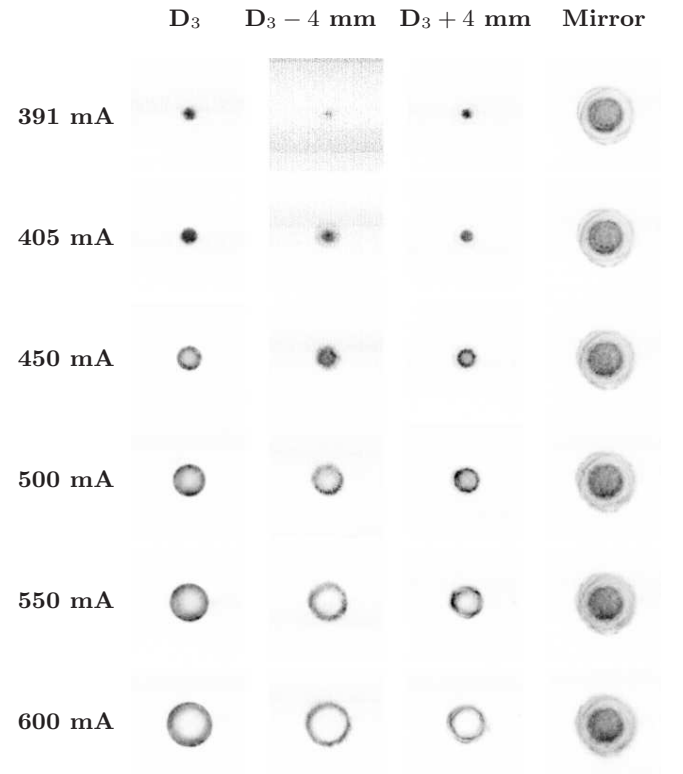


FIG. 5. Far field intensity distribution of the VCSEL with feedback from a VBG at different currents. Left column: D_3 at self-imaging distance; center columns: D_3 too short or too large by 4 mm; right column: Feedback with plane mirror.

This feature can be much better investigated in far field images. The sequence depicted in the leftmost column of Fig. 5 illustrates that the emission is very much dominated by a single ring with negligible background, i.e. only a single transverse wavenumber is lasing. The solitons start to emit on axis and the wavenumber increases monotonically with increasing current. We are going to do a quantitative investigation at the end of Sect. IV.

If the distance D_3 is changed away from the self-imaging condition the far-field images do not show a significant change except for quantitative corrections to the wavenumber (analyzed in more detail in Sect. V), but the near-field images do. For a longer cavity (+4 mm) we observe a ‘defocusing’ effect, i.e., the emission is shifting towards the boundaries of the aperture, especially at

high currents. Inversely, for a too short cavity -4 mm the pattern seems to be ‘focused’, i.e. it contracts towards the center of the device.

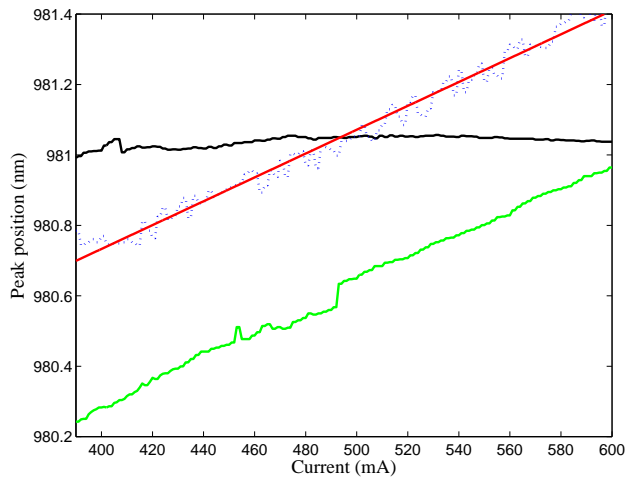


FIG. 6. (Color online) Black solid line: Frequency shift of one mode of the VCSEL with feedback of a VBG ($M = 6.25$). Green solid line (light grey in print): feedback by a plane mirror. Blue dashed line (grey in print): Free Running Laser (FRL) at 69°C . Red solid line (dark grey in print): Fit to the FRL.

Finally, Fig. 6 gives an indication of the change of emission wavelength with increasing current. The free-running laser shows an approximately linear increase with a rate of 0.0035 nm/mA device. This is due to Joule heating. The VCSEL with feedback shows a corresponding behavior, whereas the emission wavelength of the VCSEL with feedback is essentially locked to one value (within 0.06 nm) given by the peak reflection of the VBG. This matches qualitatively the observations in EEL discussed before. A closer inspection shows that the wavelength is in tendency increasing, by about 0.06 nm, at the beginning (the soliton area) and then slowly decreasing (by about 0.02 nm).

IV. INTERPRETATION

The resonance condition for a VCSEL cavity are identical to the ones of a plano-planar Fabry-Perot cavity in diverging light and were investigated in detail in [11, 13]. The dispersion relation of plane waves with a transverse wavenumber q in the VCSEL is given by [11, 13]:

$$q_{\text{VCSEL}} = \sqrt{\frac{8\pi^2 n_0 n_{gr} (\lambda_c - \lambda)}{\lambda^3}} = a\sqrt{\Delta\lambda}, \quad (1)$$

where n_0 is an average refractive index of the VCSEL and n_{gr} is the group index, λ is the vacuum wavelength of the emission and λ_g the vacuum wavelength of the longitudinal resonance. If the wavelength of the emission is

fixed by the VBG, as indicated by Fig. 6, and the longitudinal resonance shifts due to the Joule heating, different transverse wavenumbers should come into resonance with the feedback starting with those at $q = 0$. This situation is schematically depicted in Fig. 7. $\omega_g = 2\pi c/\lambda_g$ represent the grating frequency, $\omega_c = 2\pi c/\lambda_c$ the longitudinal resonance of the cavity, which decreases with increasing temperature or current. Due to the dispersion relation of the VCSEL, one expects a selection of not only wavelength, but also of transverse wavenumber, i.e. the emission should correspond to a ring in far field, which is exactly what we observed in Fig. 5. The emission angle should increase monotonically with current. Quantitatively, we expect an increase as the square root of the detuning of the VCSEL cavity, which we will investigate below. We mention that close to threshold, around $q = 0$, nonlinear frequency shifts play a role leading to the possibility of bistability of solitons: Reducing the frequency gap between grating and VCSEL resonance increases the intensity, which reduces the carrier density, increases the refractive index and thus red-shifts the cavity resonance further. This positive feedback can create an abrupt transition to lasing [7, 12, 14] and can explain also the variation in wavelengths in the range below 420 mA in Fig. 6. If the cavity resonance condition is not quite homogenous, this takes place at different current levels, which can explain that the VCSEL starts to lase locally at the locations where the resonance is most ‘reddish’, i.e. closest to the grating and then slowly fills up as obvious in the near field images (Fig. 3, left column). We propose to use this relationship to provide a mapping of the disorder of the cavity resonance [15].

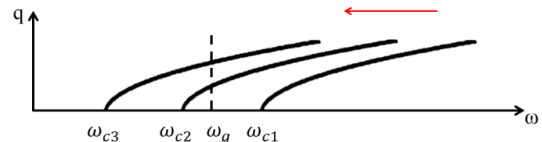


FIG. 7. Mechanism for selecting the transverse wavenumber. ω_g : grating frequency. ω_{c1} : VCSEL frequency at low current. ω_{c2} : VCSEL frequency at higher current. ω_{c3} : VCSEL frequency at high current.

The small remaining frequency shift observed at high currents (larger than 420 mA) in Fig. 6 is due to the fact that the dispersion curve of the VBG is not straight. That curvature means that there is a small difference between the operating wavelength of the device and the intercept as shown schematically in Fig. 8.

From the condition that the phase shift in a single layer of the VBG should remain $\pi/4$ also at oblique incidence, the dispersion relation of the VBG can be expressed as:

$$q_{\text{VBG}} = M\sqrt{\frac{8\pi^2 n^2 (\lambda_g - \lambda)}{\lambda^3}} = b\sqrt{\Delta\lambda} \quad (2)$$

with λ_g being the peak reflection wavelength of the VBG and n the refractive index of the glass host. From Eq. 2, one can see that if the telescope magnification M is increased then the dispersion curve will straighten up thus reducing the frequency shift. By equating (1) and (2), one obtains for $\lambda_g \leq \lambda_c$ the emission wavelength

$$\lambda = \frac{\lambda_g - \frac{a^2}{b^2}\lambda_c}{1 - \frac{a^2}{b^2}} = \lambda_g - \frac{\frac{a^2}{b^2}(\lambda_c - \lambda_g)}{1 - \frac{a^2}{b^2}} \quad (3)$$

For $M = 6.25$ and for a shift of λ_c by $0.0035\text{nm}/\text{mA} \times 210\text{mA} = 0.735\text{nm}$, we have $\lambda = \lambda_g - 0.10\text{ nm}$ which is on the order of – though somewhat larger – what we observe in Fig. 6.

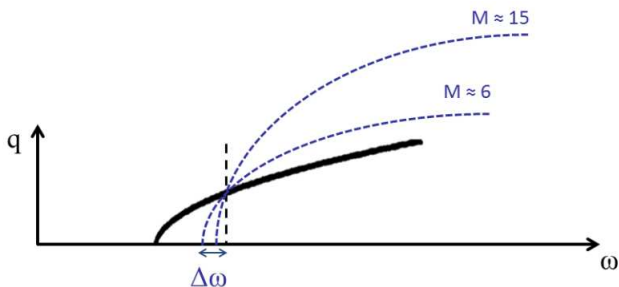


FIG. 8. Effect of the magnification M on the dispersion curve of the VBG. $M \approx 6$ corresponds to the short cavity whereas $M \approx 15$ corresponds to the long cavity. $\Delta\omega$ corresponds to a frequency shift between ω_g and the emission frequency.

To test the prediction of Eq. 3, the same experiment has been done with a second telescope arrangement i.e. a long cavity with $f_2 = 125\text{ mm}$ ($M \approx 15$) and Fig. 9 illustrates the shift in frequency of the VCSEL with this external cavity setup. The shift is barely noticeable and within the accuracy range of our equipment it is not possible to quantify it. From Eq. 3 one expects to have $\lambda = \lambda_g - 0.02\text{ nm}$ with $M = 15.6$. This result is in good agreement with our experimental observation that the curve is essentially flat beyond the soliton region (up to about 430 mA). The remaining variations are below the limit of the accuracy of our OSA (about 0.03 nm relative accuracy within a single run). These results confirm the presence of frequency locking when feedback is provided from a VBG and also that the remaining frequency shift depends on the magnification factor of the external cavity. For large magnification ($M \gg 1$), $b \gg a$, one finds $\lambda \approx \lambda_g$, i.e. perfect locking because the dispersion relation of the VBG approaches a vertical line.

As derived in the previous section, the wavenumber of the emission should follow a square root behavior with detuning. Based on data like the ones obtained in Fig. 5 this can be checked quantitatively and the results are shown in Fig. 10a, which shows indeed a nice square-root behavior with a scaling exponent of 0.502 with a negligible parameter error (on the order of 3×10^{-3}) and a high-fidelity regression coefficient ($R^2 = 0.9989$) returned by the nonlinear fitting code.

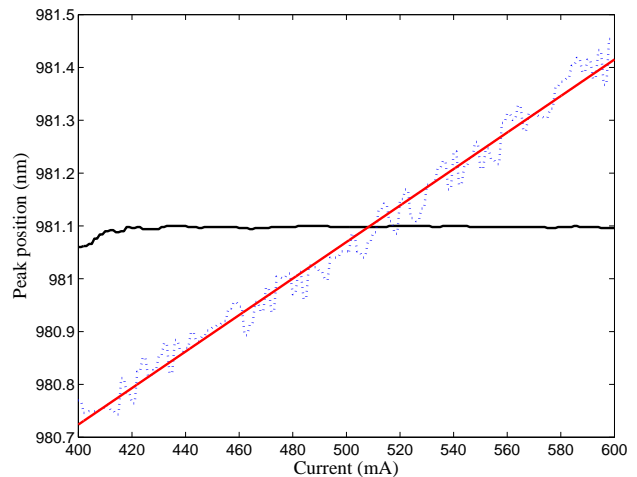


FIG. 9. (Color online) Black solid line: Frequency shift of the VCSEL with feedback of a VBG ($M = 15.6$). Blue dashed line (light grey in print): FRL at 16°C . Red solid line (grey in print): Fit to the FRL.

V. EFFECTS OF DEVIATION FROM SELF-IMAGING

By these investigations, the effect of the VBG on wavelength locking is quite clear but the influence of the distances between the intra-cavity lenses (e.g. D_2 or D_3) remains to be investigated. For example, Figs. 3 and 5 clearly indicate that D_3 has an influence on the spatial structures.

As shown in Fig. 1, a self imaging cavity is characterized by three distances. The first one is the distance D_1 between the laser and the collimation lens. It is found by adjusting the position of the lens until the divergence of the beam is minimal. The second distance D_2 is the distance separating both lenses also referred as the intra-cavity distance in the following; ideally it is $(f_1 + f_2)$. The last distance is the distance D_3 separating the second lens and the VBG. It is determined by moving the VBG until the near field image of the VCSEL has the sharpest boundaries. As indicated, matrix theory indicates that D_2 is not influencing the imaging condition for the intensity distribution. Since D_2 is hence the most poorly defined one (in the sense that there is no obvious alignment criterion like for D_1 , D_3) we first turn our attention to it.

Fig. 10b shows a dispersion relation similar to the one in a) but obtained at $D_2 = 78\text{ mm}$, away from the self-imaging condition. Though the data still seem to follow roughly a square-law like behavior, they are more scattered and the lower quality of the fit is evidenced also by reduction of the regression coefficient to $R^2 = 0.9845$ and the parameter error returned is 11×10^{-3} . The scaling exponent turns out to be slightly different from 0.5, e.g. 0.479 in Fig. 10b. This scattered behavior combined with a reduction of the fitting quality and a deviation of the scaling exponent from 0.5 is typical also for other

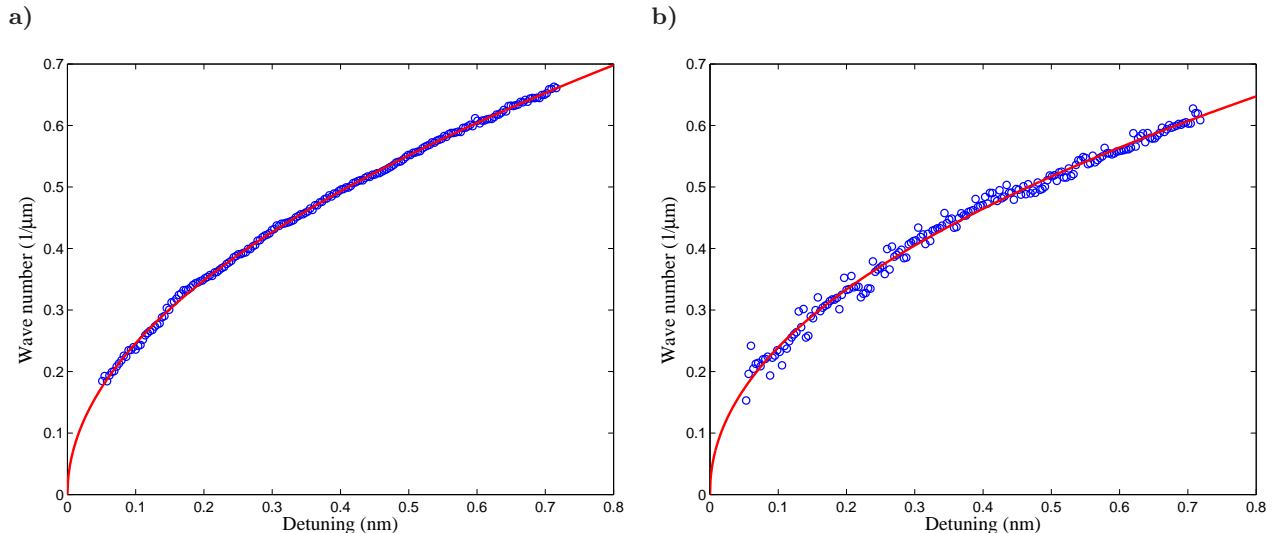


FIG. 10. Transverse wave number of the emission versus detuning between emission wavelength and longitudinal resonance (crosses represent data points and solid lines fits). a) For $D_2=70.5$ mm leading to a scaling exponent $s = 0.502$; b) for $D_2=78$ mm leading to a scaling exponent $s = 0.479$. These plots are produced by finding the intercept I_0 and the scaling exponent s using a fitting function $q(I) = c(I - I_0)^s$. The intercept I_0 then corresponds to the zero detuning condition. Starting from that the rate of 0.0035 nm/mA is applied as a coefficient to define the detuning scaling, which is used to plot the fitting curve (red curve in the figure above). The program also returns the R^2 value for the fit.

distances D_2 different from $D_2 = 70.5$ mm. For example, for $D_2 = 74$ mm, the scaling exponent is 0.508 and $R^2 = 0.9874$.

We also notice that there is an enhanced tendency for slight variations of the details of the patterns (not the basic structure) from run to run away from $D_2 = 70.5$ mm. Hence we report results averaged over three runs in Tab. I, which summarizes the effect of the intra cavity distance on the scaling exponent over a larger range. Fig. 11 illustrates the same results graphically. The first observation is that in general the averaged scaling exponent is oscillating around 0.5 with a tendency to larger values for smaller distances, but that there are actually two positions at $D_2 = 74$ and 78 mm in addition to $D_2 = 70.5$ mm at which the averaged scaling exponent is again close to 0.500 . However, as stated already above, the quality of the fits is lower and there is a larger variation between runs which we characterize by the standard deviation σ of the scaling exponents returned for the different runs (Tab. I, last row).

In order to get further insight in the nature of these deviations and variations, we analyzed the width of the ring in Fourier space as a measure of the quality of wavenumber selection (Tab. I, 2nd row and Fig. 11, dashed line). It has a minimum around $D_2 = 70.5$ mm, i.e. the anticipated self-imaging condition, and increases, except for one exception interpreted as scatter, monotonically away from it. In particular, at 70.5 mm the ring is narrower than at both 74 mm and 78 mm (see also the width in Tab. I). These observations reinforce our expectation that $D_2 = 70.5$ mm is the self-imaging position.

This behavior can be understood by the ABCD-matrix for the round-trip through the external cavity if $D_2 =$

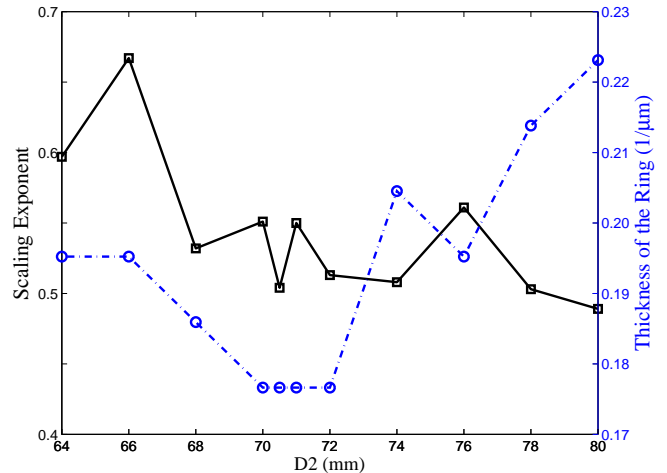


FIG. 11. Black solid line: Scaling exponent vs. D_2 . Blue dashed line: Thickness of the ring in far field vs. D_2 .

$f_1 + f_2 + x$, which reads

$$M_2 = \begin{pmatrix} 1 & 0 \\ -\frac{2}{f_1^2} x & 1 \end{pmatrix}. \quad (4)$$

A small mistuning x leads to a change of phase curvature or ray angle for the returning light. Hence the spatial Fourier spectrum broadens. Hence we conclude that $D_2=70.5$ mm corresponds to the self-imaging distance. It is also within ± 0.2 mm of the best estimate we can give on the expected cavity length from the dispersion data and the knowledge of the principal planes available for the lenses used.

TABLE I. Effect of D_2 on the scaling exponent. Three rounds of data taking averaged. The data for both 70.5 and 72 are actually based on nine runs. The width of the ring in far field is given at 500 mA.

Distance D_2 (mm)	64	66	68	70	70.5	71	72	74	76	78	80
Scaling Exponent	0.597	0.667	0.532	0.551	0.504	0.550	0.513	0.508	0.561	0.503	0.489
Width ($1/\mu\text{m}$)	0.195	0.195	0.186	0.176	0.176	0.176	0.176	0.204	0.195	0.214	0.223
Intersect (mA)	389	381	395	392	395	393	396	391	384	394	397
St. deviation σ	0.022	0.011	0.013	0.011	0.002	0.032	0.022	0.010	0.022	0.043	0.009

In order to confirm that, another experiment has been set up to study the cavity in details. It consists of the same telescope with the exact same optics (a collimation lens, a focusing lens and a beam splitter). A tunable laser is coupled into a single mode fibre. The collimated output beam is then injected into the telescope from the side with the larger focal length lens. One should expect that the beam coming out of the telescope at the collimation lens has the smallest beam divergence if the intra-cavity distance is right and indeed best collimation is found within ± 0.2 mm of $D_2=70.5$ mm, which is considered to be the accuracy of the distance measurement.

Finally, we discuss the influence of D_3 on the pattern formation. Fig. 12 indicates that it also has an influence on the scaling exponent as well as on the manifestation of structures. We noticed also in Fig. 3 that for a too long cavity the near field seems to be pushed to the perimeter, whereas for a short cavity it seems to contract inwards. The boundaries are not as sharp and well defined. Again these features can be understood by ABCD-matrix theory, which gives for $D_3 = f_2 + x$ a round trip matrix of

$$M_2 = \begin{pmatrix} 1 & \frac{2f_1^2}{f_2^2} x \\ 0 & 1 \end{pmatrix}, \quad (5)$$

i.e. the system is not imaging any more. For a ray emitted at a radius r at an angle Θ , the returning rays hits at

$$r' = r + \frac{2f_1^2}{f_2^2} \Theta x. \quad (6)$$

This means that for $x > 0$ (too long cavity), the emission is pushed outwards, whereas for $x < 0$ (too short cavity) it is pushed inward. This is the tendency observed in the experiment. Note that the angle Θ does not change very much.

VI. CONCLUSION

We established that VBGs work as wavelength lockers for VCSELs as well as for EEL lasers for which they are of significant importance for wavelength and modal control. VCSELs have already a lower temperature dependence than EEL because their wavelength shift is determined by the cavity shift of about 0.1 nm/K (GaAs based devices) compared to the gain shift of 0.2-0.3 nm/K relevant

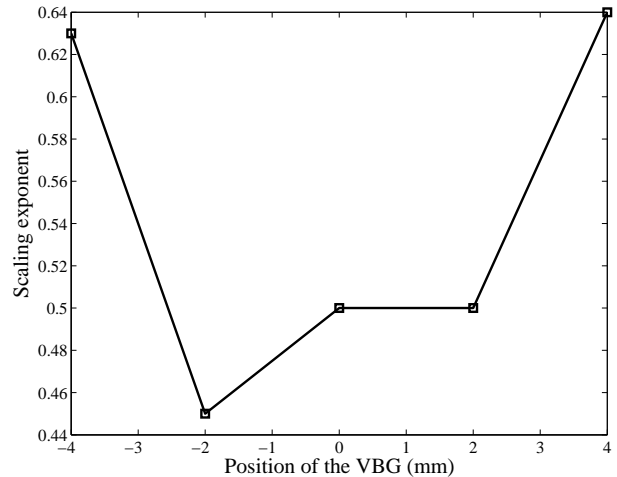


FIG. 12. Scaling exponent as function of D_3 . The 0 position indicates self imaging position and negative sign means that the VBG is moved towards the telescope. Inversely, the positive sign means that the VBG is moved away from the focusing lens.

to EEL. Nevertheless, an external VBG can decrease this shift even more and the fidelity increases with increasing magnification of the imaging system, unfortunately increasing the foot print of the system.

For increasing temperature or current, the on-axis modes come into resonance first and here phase-amplitude coupling leads to the possibility of bistability [14] and, via self-focusing, soliton formation [7, 8, 12]. Beyond threshold, we can stabilize single-wavenumber and narrow bandwidth emission with fairly high fidelity. These structures might find applications where ring-shaped foci are desired. The radius of the ring can be tuned by current (or temperature). This feature constitutes an important difference between VCSELs and EEL and stems from the fact that VCSELs are intrinsically single-longitudinal mode devices. Hence the wavelength locking is accompanied by an increase in mode order (transverse wavenumber) for increasing temperature (induced either directly via the ambient temperature or via Joule heating). In contrast, for an EEL consequent longitudinal orders will shift into resonance and hence the modal distribution will contain the mixture of low-order and high-order modes typical for broad-area EEL, but the average mode order won't be increasing so much

as in the VCSEL.

We also analyzed the effect of deviations of the external cavity from the self-imaging condition. It turns out that the system is remarkably insensitive to deviations even in the mm range for a cavity length in the 100 mm range. This is good news for the robustness of experimental conditions. We remark that we consider the self-imaging condition to be attractive for these kind of experiments because it allows for best feedback efficiency in terms of amplitude and phase. An autocollimation setup using only the collimation lens (as in [4, 5]) not only introduces an image inversion (relevant for Gauss-Hermite modes for example), but due to the shortness of the focal lengths of typical collimation lenses, it is also likely that the length of the external cavity is larger than the perfect telescope length (an imperfect D_2 in our terminology).

Hence, there is a phase curvature of the returning beam for Gaussian modes and a chance of ray direction for Fourier modes and as a result an imperfect interference with the cavity mode. Deviations from the self-imaging conditions make it also more difficult to model the returning field distribution, though in principle methods like the Collins-integral are available, of course [16].

ACKNOWLEDGEMENTS

Y.N. is supported by an EPSRC DTG. We are grateful to W.J. Firth and Jesus Jimenez-Garcia for useful discussions and to R. Jaeger (Ulm Photonics) for supplying the devices.

-
- [1] B. L. Volodin, S. V. Dolgy, E. D. Melnik, E. Downs, J. Shaw, and V. S. Ban, *Opt. Lett.* **29**, 1891 (2004).
 - [2] M. Maiwald, A. Ginolas, A. Müller, A. Sahm, B. Sumpf, G. Erbert, and G. Tränkle, *IEEE Photon. Tech. Lett.* **20** (2008).
 - [3] F. Kroeger, I. Breunig, and K. Buse, *Appl. Phys. B* **95**, 603608 (2009).
 - [4] F. Marino, S. Barland, and S. Balle, *IEEE Photon. Technol. Lett.* **15**, 789 (2003).
 - [5] Y. K. Chembo, S. K. Mandre, I. Fischer, W. Elsässer, and P. Colet, *Phys. Rev. A* **79**, 013817 (2009).
 - [6] M. Schulz-Ruhtenberg, Y. Tanguy, K. F. Huang, R. Jäger, and T. Ackemann, *J. Phys. D: Appl Phys.* **42**, 055101 (2009).
 - [7] N. Radwell and T. Ackemann, *IEEE J. Quantum Electron.* **45**, 1388 (2009).
 - [8] T. Ackemann, G.-L. Oppo, and W. J. Firth, *Adv. Atom. Mol. Opt. Phys.* **57**, 323 (2009).
 - [9] M. Grabherr, R. Jäger, M. Miller, C. Thalmaier, J. Herlein, and K. J. Ebeling, *IEEE Photon. Technol. Lett.* **10**, 1061 (1998).
 - [10] M. Grabherr, M. Miller, R. Jäger, R. Michalzik, U. Martin, H. J. Unold, and K. J. Ebeling, *IEEE J. Sel. Top. Quantum Electron.* **5**, 495 (1999).
 - [11] M. Schulz-Ruhtenberg, Y. Tanguy, R. Jäger, and T. Ackemann, *Appl. Phys. B* **97**, 397 (2009).
 - [12] Y. Tanguy, T. Ackemann, W. J. Firth, and R. Jäger, *Phys. Rev. Lett.* **100**, 013907 (2008).
 - [13] M. Schulz-Ruhtenberg, I. Babushkin, N. A. Loiko, T. Ackemann, and K. F. Huang, *Appl. Phys. B* **81**, 945 (2005).
 - [14] A. Naumenko, N. A. Loiko, M. Sondermann, K. F. Jentsch, and T. Ackemann, *Opt. Commun.* **259**, 823 (2006).
 - [15] T. Ackemann, N. Radwell, and Y. Noblet, (2012), submitted to *Opt. Lett.*
 - [16] A. M. Dunlop, E. M. Wright, and W. J. Firth, *Opt. Commun.* **147**, 393 (1998).